

Temperature and material flow in one-step double-acting friction stir welding process of aluminum alloy: Modeling and experimental

Eko Prasetya Budiana^{1*}, Sekar Gading Happy Hapsari¹, Essam R. I. Mahmoud², Triyono^{1*}

¹ Department of Mechanical Engineering, Universitas Sebelas Maret, Surakarta 57126, Indonesia

² Department of Mechanical Engineering, Islamic University of Madinah, Medina 42351, Saudi Arabia

✉ ekoprasetya@staff.uns.ac.id // triyono74@staff.uns.ac.id



Highlights:

- Hydrogen solubility mismatch between liquid and solid aluminum in fusion welding causes porosity, compromising weld quality.
- One-step double-side Friction Stir Welding (FSW) offers a time-efficient solution for thick aluminum by applying two synchronized tools, enabling simultaneous dual-surface welding.
- CFD-based simulation accurately predicted temperature and material flow, validated by structural analysis and yielding a low error margin of 4.07%.

Abstract

Aluminum, known for its lower density compared to steel, is widely used in various applications. Welding is often required to form aluminum into technical structures. However, when fusion welding is used, it can lead to porosity in the weld. This occurs due to the significant difference in hydrogen gas solubility between liquid and solid aluminum, which traps hydrogen gas within the weld metal. Friction Stir Welding (FSW), a solid-state welding technique, has been proven to minimize porosity. However, for thick structures, FSW poses challenges, as welding must be done on both sides, increasing the welding time. To overcome this limitation, FSW has been modified into a one-step double-side FSW process, where two tools simultaneously work on both surfaces of the workpiece. This creates a unique condition with two heat sources and two stirring motion sources. To understand the temperature distribution and material flow in this process, modeling was conducted using Computational Fluid Dynamics (CFD). The upper and lower tools in the one-step double-side FSW process operate under identical conditions: a rotation speed of 1500 rpm, a welding speed of 30 mm/min, and a tilt angle of 0 degrees. The aluminum plate is treated as fluid, while the tools are considered solid in the model. The results of the temperature distribution modeling were validated against published studies, and the material flow was verified through macro- and microstructural observations of the cross-section. The validation showed that the model is accurate, with an error of only 4.07%.

Keywords: One-step double-side FSW; Aluminum; Material flow; Temperature distribution; Modeling

Article info

Submitted:
2025-01-09

Revised:
2025-03-10

Accepted:
2025-04-15



This work is licensed under a Creative Commons Attribution-NonCommercial 4.0 International License

Publisher

Universitas Muhammadiyah
Magelang

1. Introduction

Aluminum is extensively used in various industries due to its low density compared to steel, making it ideal for lightweight applications. However, pure aluminum lacks sufficient strength for structural applications and is therefore alloyed with other elements to enhance its mechanical properties [1], [2], [3], [4]. Due to its high strength, excellent formability, and superior corrosion resistance, aluminum and its alloys are widely employed in aerospace, railway, maritime, automotive, and large structural applications [5], [6], [7].

Traditionally, aluminum is joined using fusion welding methods, which involve melting and re-solidifying the material to create a joint [8], [9]. However, fusion welding of aluminum often leads to porosity defects due to the material's high hydrogen solubility in the liquid state and limited solubility in the solid state. As the metal solidifies, trapped hydrogen gas forms pores within the weld, compromising toughness, fatigue resistance, and ductility [10], [11], [12], [13]. Additionally, fusion welding can accelerate the corrosion rate of the weldment [14]. To address these challenges, Friction Stir Welding (FSW) has emerged as a promising alternative. Unlike fusion welding, FSW is a solid-state process that avoids melting, thereby minimizing porosity and improving joint quality [15]. In FSW, a rotating tool generates frictional heat, softening the workpiece material and mechanically stirring it to create a metallurgical bond [16].

Despite its advantages, conventional FSW is associated with uneven joint strength due to inconsistent heat distribution. Additionally, when welding thicker materials, performing the process on both surfaces is often necessary, increasing welding time and requiring complex fixture setups. To overcome these limitations, One-Step Double-Acting Friction Stir Welding (ODFSW) has been developed, utilizing two tools to weld both surfaces simultaneously. This method enhances efficiency by reducing setup complexity and overall welding time while improving heat input uniformity [17], [18].

The quality of FSW joints is highly dependent on key process parameters such as tool rotational speed, pin geometry, axial force, tilt angle, welding speed, and plunge depth [19], [20], [21]. Additionally, some studies suggest that stirring time also influences defect formation during the solidification of molten aluminum [22]. These parameters govern the thermomechanical conditions in the stirring zone, influencing material flow and determining the final weld properties. Optimal conditions ensure defect-free joints with refined grain structures and superior mechanical performance, whereas suboptimal conditions may lead to defects that compromise structural integrity [18], [19]. Material flow behavior is particularly critical, as improper flow can result in tunnel defects, kissing bonds, and void formations, affecting weld quality. Given its importance, extensive research has been conducted to analyze temperature distribution and material flow in conventional FSW using both experimental and numerical approaches [23], [24], [25].

Comprehensive reviews, such as those by Ambrosio et al. [24], Sharma et al. [25], and Youlia et al. [26], have provided valuable insights into heat distribution and material flow in conventional FSW. However, research on these aspects in one-step double-acting FSW remains limited. The unique dual-configuration system in ODFSW introduces two heat sources and two stirring mechanisms operating simultaneously, leading to more complex thermal gradients and material flow patterns compared to conventional FSW, which utilizes a single heat and stir source. Understanding these complexities is crucial for optimizing process parameters and improving weld quality. This study aims to address existing research gaps by analyzing material flow, microstructural evolution, and defect formation in one-step double-acting FSW. By providing a deeper understanding of the complex interactions occurring during this process, this research contributes to the optimization of ODFSW parameters and the advancement of weld quality assessment techniques. The findings of this study will offer valuable insights for industrial applications requiring high-quality aluminum welds, helping to refine welding strategies and enhance manufacturing efficiency.

2. Numerical Method

The CFD simulation software is employed to analyze steady-state heat flow using the conjugate heat transfer method, which couples fluid flow with heat transfer. The simulation flowchart is presented in [Figure 1](#). In this 3D model, the material flow region undergoing severe plastic deformation is treated as a highly viscous, non-Newtonian fluid moving past the rotating tool, while the remainder of the workpiece is considered solid. A sliding-sticking contact condition is assumed between the tool and workpiece, allowing both friction and plastic deformation to generate heat at their interfaces.

In this study, a finite volume model is used to simulate the process. The model consists of two main geometric domains: the tool and the workpiece. The workpiece domain includes two blocks, each measuring 200 mm x 100 mm x 6.5 mm. The cylindrical FSW tool features a shoulder with a diameter of 18 mm and a height of 183 mm, along with a pin that has a diameter of 4 mm and a height of 3 mm. The tool is incorporated into the model as a wall, with a 0.15 mm indentation in the weld plate caused by the plunging force during welding. The workpiece material is AA6061, while the tool is made of AISI H13 tool steel. [Table 1](#) provides the physical and thermal properties

of AA6061 and AISI H13 tool steel, and **Figure 2** illustrates the dimensions of the workpiece, tool, and joint configuration.

The FSW process is governed by the principles of mass, momentum, and energy conservation. Given that the material's mass remains constant, the mass conservation equation can be expressed as following Eq. (1).

$$\frac{\partial u}{\partial x} + \frac{\partial v}{\partial y} + \frac{\partial w}{\partial z} = 0 \quad (1)$$

where u , v , and w are the velocities in the x , y , and z directions, respectively. The conservation of momentum is described by the Navier-Stokes equation as following Eq. (2) to Eq. (4). where g_x , g_y , and g_z are the forces in x , y , and z directions, respectively; p is the static pressure of the flow field; μ is the viscosity of fluid, and ρ is the density of material. The energy conservation equation is given by Eq. (5). where C_p is the specific heat of material, k is the thermal conductivity of material, \dot{q} is heat flux and T is the temperature of fluid.

The simulation employed hexahedral meshing to match the block-like shape of the geometry. The MultiZone method was also used to accommodate the two distinct material domains within the geometry, enabling precise definition of different material properties. Element sizes were set according to default settings, with a maximum size of 20.5 mm in regions distant from the tool and a minimum size of 0.1 mm in critical areas near the tool. This meshing process generated 2,639 nodes and 5,008 elements, as illustrated in **Figure 3**.

The boundary conditions for the geometry include an inlet, outlet, and wall, as shown in **Figure 4**, designed to closely replicate the one-step double-acting FSW (ODFSW) process. The upper and lower tools are assumed to move along the z -axis, from negative to positive, which drives the material flow in the opposite direction—from positive to negative along the z -axis. The upper tool is positioned at zero on the y -axis, while the lower tool is positioned in the negative y direction. Both tools rotate counterclockwise. The inlet velocity matches the welding speed of 30 mm/min, with an initial temperature of 293 K. At the outlet, the pressure is set to 0 Pa. A convection coefficient of 30 W/m² is applied to the top and side walls of the workpiece, and a backing plate beneath the workpiece in the ODFSW process provides a higher convection coefficient of 300 W/m² on the bottom wall. The tool temperature is set to 80% of the melting point of AA6061 [25].

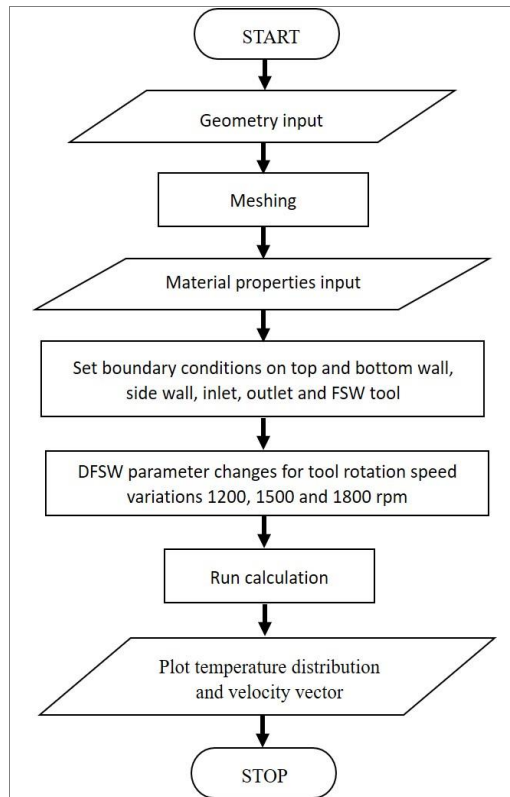


Figure 1.
Flowchart of friction stir welding simulation

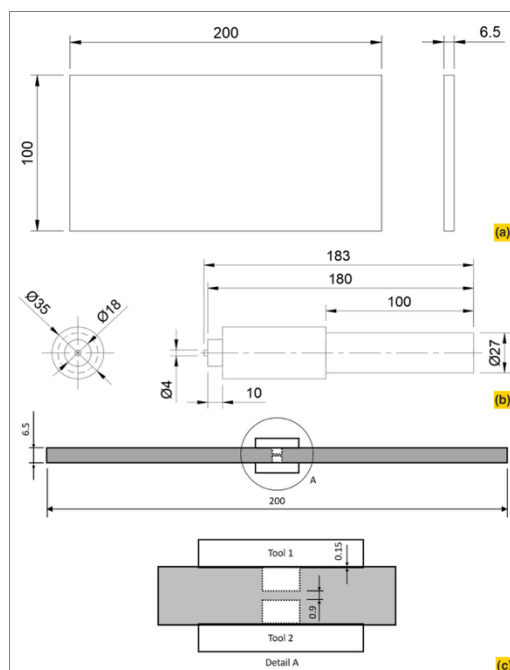


Figure 2.
The dimension of:
(a) Workpiece;
(b) Tool;
(c) Joint configuration

Table 1.
Physical and thermal properties of AA6061 and AISI H-13 [25], [27]

Properties	AA6061	AISI H-13
Density	2.7 g/cm ³	7.8 g/cm ³
Melting point	582 °C	1427 °C
Thermal conductivity	167 W/m. -K	28.6 W/m. -K
Specific heat capacity	0.869J/g.°C	0.460J/g.°C
Viscosity	0.0013 kg/m.s	

$$\rho \left(u \frac{\partial u}{\partial x} + v \frac{\partial u}{\partial y} + w \frac{\partial u}{\partial z} \right) = \rho g_x - \frac{\partial p}{\partial x} + \mu \left(\frac{\partial^2 u}{\partial x^2} + \frac{\partial^2 u}{\partial y^2} + \frac{\partial^2 u}{\partial z^2} \right) \quad (2)$$

$$\rho \left(u \frac{\partial v}{\partial x} + v \frac{\partial v}{\partial y} + w \frac{\partial v}{\partial z} \right) = \rho g_y - \frac{\partial p}{\partial y} + \mu \left(\frac{\partial^2 v}{\partial x^2} + \frac{\partial^2 v}{\partial y^2} + \frac{\partial^2 v}{\partial z^2} \right) \quad (3)$$

$$\rho \left(u \frac{\partial w}{\partial x} + v \frac{\partial w}{\partial y} + w \frac{\partial w}{\partial z} \right) = \rho g_z - \frac{\partial p}{\partial z} + \mu \left(\frac{\partial^2 w}{\partial x^2} + \frac{\partial^2 w}{\partial y^2} + \frac{\partial^2 w}{\partial z^2} \right) \quad (4)$$

$$\rho \cdot Cp \left(u \frac{\partial T}{\partial x} + v \frac{\partial T}{\partial y} + w \frac{\partial T}{\partial z} \right) = \frac{\partial}{\partial x} \left(k \frac{\partial T}{\partial x} \right) + \frac{\partial}{\partial y} \left(k \frac{\partial T}{\partial y} \right) + \frac{\partial}{\partial z} \left(k \frac{\partial T}{\partial z} \right) + \dot{q} \quad (5)$$

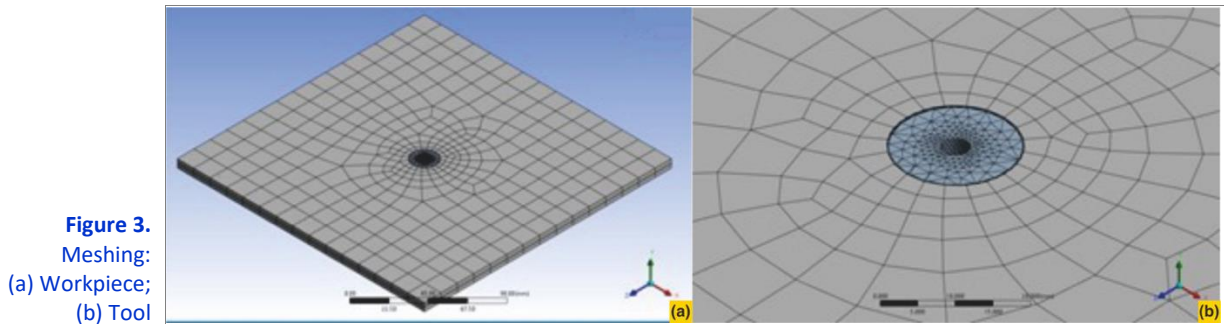


Figure 3.
Meshing:
(a) Workpiece;
(b) Tool

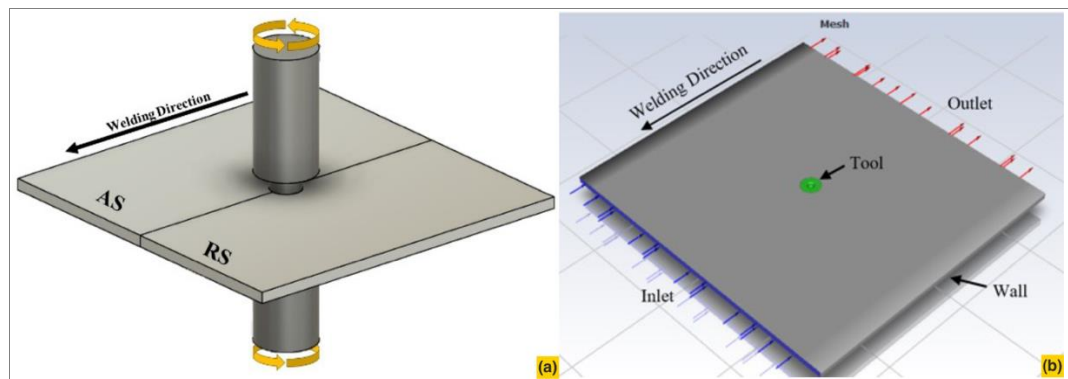


Figure 4.
Boundary conditions:
(a) Experiment;
(b) Modeling

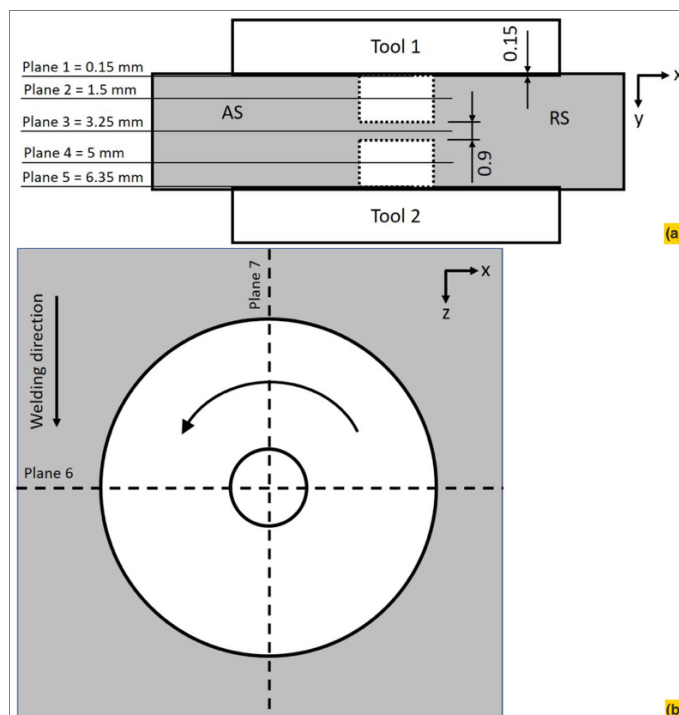


Figure 5.
Selected planes for displaying material flow velocity vectors:
(a) Depth from surface;
(b) Orientation relative to welding direction

To make the model easier to understand, data on material velocity vectors and temperature at selected planes and points will be presented. The material velocity vectors displayed are those on planes 1 through 7, as shown in Figure 5. Planes 1 through 5 are located at depths of 0.15 mm, 1.5 mm, 3.25 mm, 5 mm, and 6.35 mm from the top surface of the workpiece. Plane 6 is a cross-section perpendicular to the welding direction, while Plane 7 is parallel to it.

To construct the temperature profile, data is collected while the tool is positioned at the center of the plate during welding. On the Advanced Side (AS),

temperature readings are taken at 8 locations along the negative X-axis, spaced at intervals of 3 mm, 13 mm, 23 mm, 33 mm, 43 mm, 53 mm, 63 mm, and 73 mm. Likewise, on the Retreat Side (RS), measurements are taken at 8 corresponding points along the positive X-axis, following the same intervals.



Figure 6.
ODFSW process

3. Experimental Method

The experimental one-step double-acting friction stir welding (ODFSW) process was conducted using the same tool, material, and welding parameters as described in the previous model, ensuring consistency for validation. Figure 6 illustrates the ODFSW process, while Figure 7 shows the temperature measurement points. Temperature readings were taken at specific locations (13 mm, 23 mm, and 33 mm) from the welding line. However, measuring temperatures closer to the weld was challenging due to the size constraints of the tool and thermocouple. After welding, the samples were examined for macro- and microstructural characteristics, focusing on grain orientation to analyze material flow.

Macrostructural and microstructural observations focused on the cross-section perpendicular to the welding direction, conducted with an optical microscope. Specimens were etched following the ASTM E 407-99 Standard Practice for Microetching Metals and Alloys. This etching process involved grinding, polishing, and etching with Keller's reagent, prepared with 5 ml of HNO₃, 2 ml of HF, 3 ml of HCl, and 190 ml of H₂O.

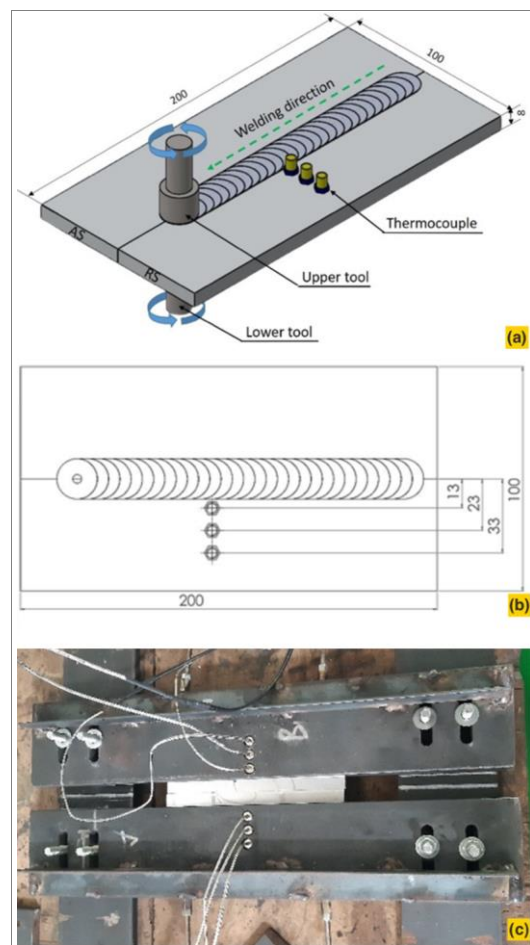


Figure 7.
Temperature measurement points:
(a) Isometrically view;
(b) Engineering drawing;
(c) Thermocouple clamping

4. Results and Discussion

4.1. Validation Method

In this study, both quantitative and qualitative validation approaches were employed to ensure the accuracy of the FSW modeling. The quantitative validation involved comparing the temperature distribution results from this study's FSW model with those from Siddiqui's study [28] and experimental measurements.

The same materials were used in all cases: AA6061 aluminum alloy as the workpiece material and high-carbon steel (HCS) as the tool material.

For validation against Siddiqui's study, temperature values were taken at specific points—3 mm, 5 mm, 7 mm, 8 mm, 10 mm, and 13 mm from the weld centerline—to ensure consistency in comparison. However, experimental temperature measurements could not be taken at these exact points due to challenges in thermocouple placement, primarily because of the tool's shoulder diameter of 18 mm. Instead, experimental temperature data were recorded at 13 mm, 23 mm, and 33 mm from the weld centerline. Figure 8 presents a comparative analysis of the temperature values obtained from both models at the selected points, as well as the experimental results. The comparison with Siddiqui's study showed an average error of 4.07% across all measured points, indicating strong agreement between the models. In contrast, the error in comparison with experimental measurements was higher, calculated at 11% across the three available points. The higher discrepancy in experimental results can be attributed to several factors, including the

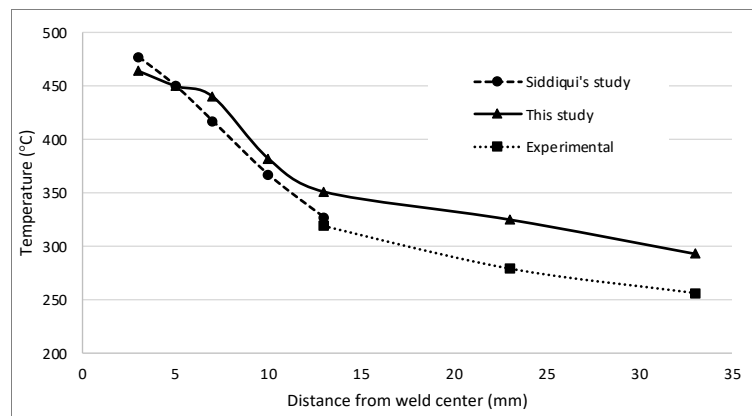


Figure 8.
Quantitative validation

response delay of the thermocouple and the high thermal conductivity of aluminum, which can lead to rapid heat dissipation and measurement variations. Despite these factors, the relatively low error rates confirm the reliability of the temperature distribution predictions in this study.

Microstructural analysis is an effective qualitative method for verifying material flow patterns in the ODFSW process, as grain orientation provides insights into the direction of material movement. In this study, microstructural observations were performed on cross-sections perpendicular to the welding direction (x-y plane). Samples were taken from five specific locations: Point 1 was positioned at the center between the two pins, Points 2 and 4 were within the Thermo-Mechanically Affected Zone (TMAZ) on the Advancing Side (AS) for the upper and lower tools, and Points 3 and 5 were within the TMAZ on the Retreating Side (RS) for both tools.

The TMAZ is a critical transition region in the friction stir welding (FSW) process, where the material undergoes significant plastic deformation due to the combined effects of the tool's rotation and translational movement. This zone plays a crucial role in determining the mechanical properties of the weld, as it bridges the relatively undeformed base material (BM) and the fully recrystallized Stir Zone (SZ) or Dynamic Recrystallization Zone (DXZ). Given its importance, samples from the TMAZ are frequently analyzed to evaluate grain structure, hardness distribution, and material flow characteristics, all of which contribute to the overall strength and structural integrity of the joint.

Understanding the material flow mechanisms in the TMAZ is particularly important, especially in regions close to the pin of the FSW tool, where intense shear forces and frictional heating are concentrated. The interaction between these forces dictates the extent of grain distortion and influences defect formation, making it essential to optimize process parameters to minimize potential weaknesses in this zone [27], [29]. Studies have shown that the material in the TMAZ is subjected to a complex flow pattern, where it is deformed but does not undergo full recrystallization. This partial transformation results in elongated and distorted grains rather than the fine, equiaxed grains observed in the SZ. Material flow in the TMAZ is primarily driven by the shear forces exerted by the rotating tool pin, combined with the thermal influence generated by frictional heating. Unlike the SZ, where dynamic recrystallization occurs due to intense plastic deformation and localized heating, the TMAZ experiences lower strain rates, preventing the formation of completely new grains. Instead, the existing grains undergo elongation and partial reorientation along the shear direction, leading to a characteristic grain structure that is distinctly different from both the BM and SZ [30], [31].

The grain orientation patterns in the TMAZ are typically anisotropic, with grains appearing stretched in the direction of material flow. This is especially evident in areas close to the advancing side of the weld, where the material undergoes greater deformation due to higher shear stresses. The retreating side, in contrast, experiences relatively lower shear forces, leading to variations in grain distortion across the TMAZ. These differences highlight the asymmetric nature of the FSW process, where the interaction between the tool, material, and process parameters influences the microstructural evolution in different regions of the weld. The thermal influence in the TMAZ is another crucial factor that affects grain structure evolution. Although the temperatures in this zone are elevated due to frictional heating, they are not sufficient to induce complete recrystallization. Instead, the grains undergo recovery processes, where some dislocations are rearranged, but the overall grain structure remains elongated rather than equiaxed. This distinguishes the TMAZ from the SZ, where the combination of heat and mechanical work is sufficient to drive full dynamic recrystallization, resulting in finer, equiaxed grains.

The location of the TMAZ adjacent to the SZ means that it is also subjected to thermal gradients, which can influence the extent of grain refinement. In one-step double-acting FSW, the downward force exerted by the tool helps improve material consolidation, but it also affects heat distribution within the weld. As a result, variations in grain structure can be observed depending

on process parameters such as tool rotational speed, welding speed, and axial force. Higher rotational speeds generally lead to increased frictional heating, which can enhance grain refinement in the TMAZ but may also promote excessive softening, reducing the overall strength of the joint. The microstructural results presented in [Figure 9](#) confirm the accuracy of the material flow model, showing strong consistency between experimental observations and numerical predictions. The alignment between these findings validates the proposed mechanism of shear-driven deformation in the TMAZ, reinforcing the understanding that this zone acts as a transition between the BM and SZ. Furthermore, the differences in grain structure between the TMAZ and SZ emphasize the need for precise control over FSW parameters to optimize weld quality.

At point 1, located between the two pins, material flow was irregular due to the complex interaction between the upper and lower pin rotations. These rotations generate opposing forces that combine with centrifugal force, creating a compressive effect that leads to a turbulent material flow pattern. The grain orientation observed at this point appears disordered, which is consistent with model predictions of turbulent flow in this area. For points 2 and 4, located in the TMAZ on the AS for the upper and lower tools, grain orientation follows a uniform pattern that aligns well with the modeled material flow direction. Here, the material flow is strong, guided by the direction of pin rotation, which creates elongated grain structures oriented toward the weld center [32]. The model's velocity vectors in [Figure 9b](#) reflect this stronger flow compared to points 3 and 5 on the RS. On the RS, represented by points 3 and 5, grain orientation remains consistent with model predictions, showing a movement toward the weld center but opposite to the AS flow direction due to pin rotation.

Besides the flow direction, the model also accurately reflects variations in material flow velocity. On the AS, stronger flow leads to more elongated grains, a result of intense plastic deformation, while on the RS, with its weaker flow, grains appear shorter. This alignment between observed and predicted flow patterns and grain structure demonstrates that material flow modeling in ODFSW effectively captures the actual welding process dynamics, making it a valuable analytical tool for optimizing and refining ODFSW techniques.

The comparative analysis between experimental microstructural observations and numerical simulation results demonstrates a strong correlation, validating the reliability of the material flow model in the One-Step Double-Acting Friction Stir Welding (ODFSW) process. At Point 1, located between the two pins, the experimental results showed irregular material flow due to the complex interaction of the upper and lower pin rotations, generating opposing forces and centrifugal effects that resulted in a turbulent pattern. This observation aligns with the simulation, which predicted chaotic velocity distributions in this region. Similarly, at Points 2 and 4, situated in the TMAZ on the Advancing Side (AS), both experimental and simulation results confirmed a strong and uniform material flow direction guided by pin rotation, leading to elongated grain structures oriented toward the weld center. The velocity vectors in the simulation accurately reflected this intensified material flow. On the Retreating Side (RS), at Points 3 and 5, experimental observations revealed

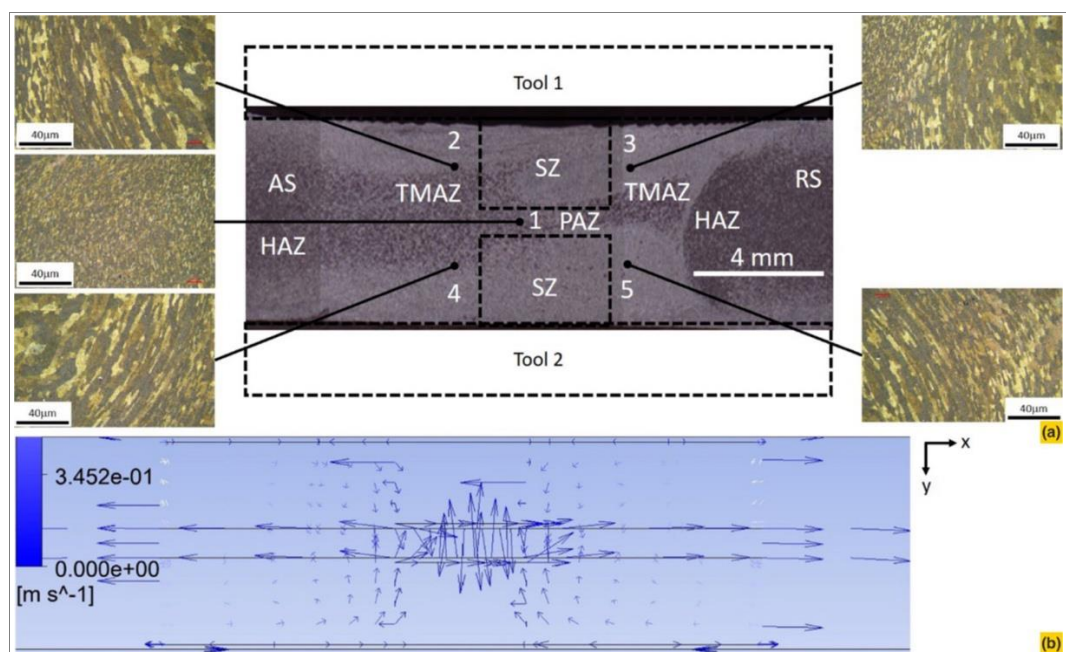


Figure 9.
Qualitative validation:
(a) Macro and
microstructure
observation;
(b) Corresponding
material flow modeling

a weaker material flow compared to the AS, with grain structures appearing shorter due to reduced plastic deformation. The simulation effectively captured this variation, demonstrating a lower flow velocity in these regions. In addition to flow direction, the simulation successfully predicted variations in material flow velocity, where the AS exhibited stronger deformation, resulting in more elongated grains, while the RS showed weaker flow, producing shorter grains. The consistency between the microstructural analysis and the numerical predictions highlights the effectiveness of the material flow model in accurately replicating the real welding process, making it a valuable tool for optimizing and refining ODFSW techniques.

The accuracy of the numerical model depends on several critical factors, including material properties, thermal boundary conditions, tool geometry, and process parameters. Material properties such as temperature-dependent thermal conductivity, specific heat capacity, and flow stress play a crucial role in determining heat generation and material flow behavior. Accurate representation of these properties ensures that the simulation closely replicates experimental results. Additionally, thermal boundary conditions, including heat transfer coefficients at the tool-workpiece interface and the surrounding environment, significantly impact the predicted temperature distribution and cooling rates. Tool geometry, particularly the pin and shoulder dimensions, affects heat generation, plastic deformation, and material flow patterns. In the present study, the use of a double-acting tool introduces additional complexity, as the interaction between the upper and lower pins influences material movement. This was observed in both the experimental and numerical results, where turbulent flow was noted between the two pins (Point 1), aligning with the model's predictions. Process parameters, such as tool rotational speed, traverse speed, and plunge depth, directly influence the accuracy of the material flow model. The quantitative validation, which compared temperature distributions with Siddiqui's model [28], demonstrated an average error of only 4.07%, confirming that the selected parameters provided reliable predictions. Furthermore, qualitative validation through microstructural analysis showed strong agreement between the predicted and observed material flow characteristics, further reinforcing the accuracy of the simulation.

4.2. Distribution of Temperature

The temperature contours for each plane, as defined in Figure 5, are illustrated in Figure 10, highlighting the thermal characteristics of the one-step double-acting FSW process. Plane 1 is positioned 0.15 mm below the top surface, while Plane 5 is located 0.15 mm above the bottom surface. Similarly, Plane 2 is situated 1.65 mm below the top surface, Plane 4 is 1.65 mm above the bottom surface, and Plane 3 lies at the plate's mid-thickness, at a depth of 3.25 mm. In the one-step double-acting FSW process, where two tools operate simultaneously on the top and bottom surfaces, Figure 10 reveals a symmetrical thermal pattern. Plane 1 corresponds to Plane 5, and Plane 2 corresponds to Plane 4, with identical temperature contours on these planes. The advancing side (AS) exhibits a more extended temperature contour compared to the retreating side (RS), reflecting higher thermal activity. Additionally, the temperature contours at the rear of the tool are broader than those at the front, aligning with

previously reported findings [33], [34].

The proximity of Planes 1 and 5 to the shoulder results in the highest peak temperature, recorded at 465.5 °C. Conversely, Plane 3, located at the plate's mid-thickness and farthest from the shoulder, experiences the lowest peak temperature of 457.5 °C. This temperature is remaining below the melting point of AA6061 alloy which indicates effective frictional heating, ensuring solid-state welding without causing localized melting. The temperature distribution across the plate thickness creates a distinctive "double-V" profile. This profile features the highest temperatures

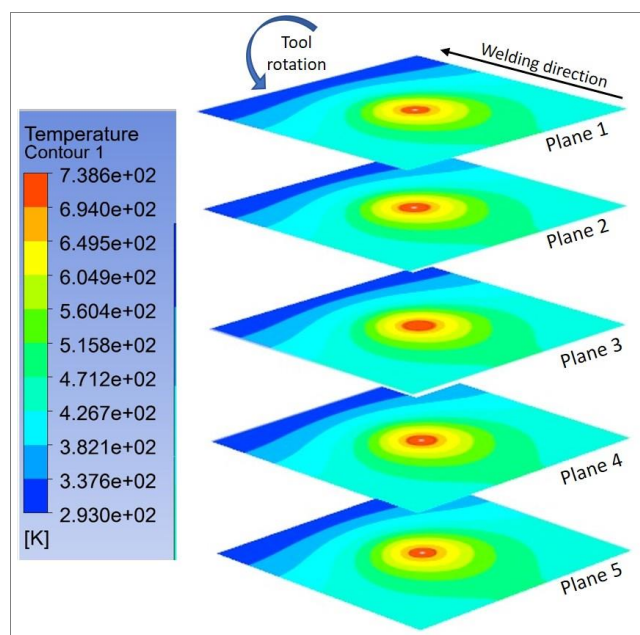


Figure 10. Temperature contour of each plane corresponding to the planes defined in Figure 4

at the outer surfaces (top and bottom), gradually decreasing toward the plate's center. This pattern is clearly visualized in the isometric view in **Figure 11**. This "double-V" thermal profile is unique compared to the conventional FSW process, where the temperature distribution typically forms a single "V" shape. In conventional FSW, the highest temperature occurs near the shoulder and diminishes with distance, with the lowest temperature observed on the surface opposite the shoulder [35], [36]. In the one-step double-acting FSW process, the dual-tool setup creates more uniform and symmetrical heating across the plate. Furthermore, the temperature contours across the plate thickness, perpendicular to the welding direction, align with prior studies indicating that the AS consistently exhibits higher temperatures and broader thermal contours compared to the RS. This behavior arises from the higher material dynamics on the AS, where the stirring action of the pin opposes the material flow caused by the tool's translational motion [36], [37], [38], [39]. **Figure 11** also illustrates the temperature distribution on a cross-section parallel to the welding direction. The "double-V" profile is evident, with the contour area at the front of the tool being narrower than that at the rear. This observation underscores the unique thermal characteristics of the one-step double-acting FSW process, distinguishing it from conventional FSW and highlighting its potential advantages in managing heat distribution and material flow.

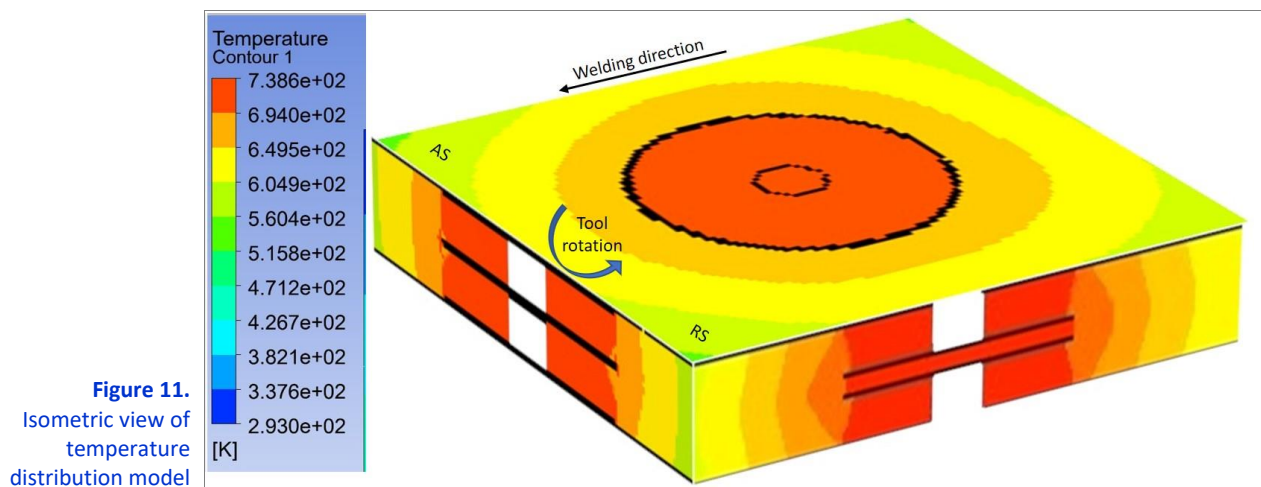


Figure 11.
Isometric view of
temperature
distribution model

4.3. Material Flow

The material flow in one-step double-acting friction stir welding (FSW) is visualized based on the temperature measurement planes in **Figure 10**, shown in **Figure 12**. Similar patterns are observed across these planes: Plane 1 corresponds to Plane 5, Plane 2 aligns with Plane 4, and Plane 3 illustrates flow at the plate's mid-thickness.

The dual heat sources, where both the upper and lower surfaces are heated by opposing rotating tools, create symmetrical velocity vector contours across the plate thickness, ensuring balanced heat input. This symmetry promotes consistent material flow and uniform deformation. In comparison, conventional FSW, which uses a single heat source, often results in asymmetrical heat distribution where exhibits more pronounced temperature gradients between the upper and lower surface [33]. This asymmetry in conventional FSW causes uneven material flow, leading to potential defects such as voids or incomplete bonding, especially in thicker plates [16], [20].

The advancing side (AS) in one-step double-acting FSW experiences more dynamic material flow due to the pin's rotation opposing the tool's movement, which generates higher temperatures and heat input. This intensifies plastic deformation, resulting in elongated and flattened grains, while the retreating side (RS) shows less pronounced deformation due to reduced heat input. Similarly, conventional FSW also exhibits temperature gradients between the AS and RS, but the differences in material flow and heat distribution are typically more pronounced, leading to greater microstructural variation across the joint.

Planes 1 and 5, located near the shoulder's frictional heat source, exhibit the highest temperatures and material flow velocities, reaching 0.43 mm/s. In contrast, the mid-thickness region at a depth of 3.25 mm experiences a significant drop in material flow velocity to 0.01 mm/s due to reduced thermal input. This flow profile contrasts with conventional FSW, which relies on a single heat source. In conventional FSW, the lowest material flow velocity is typically observed at

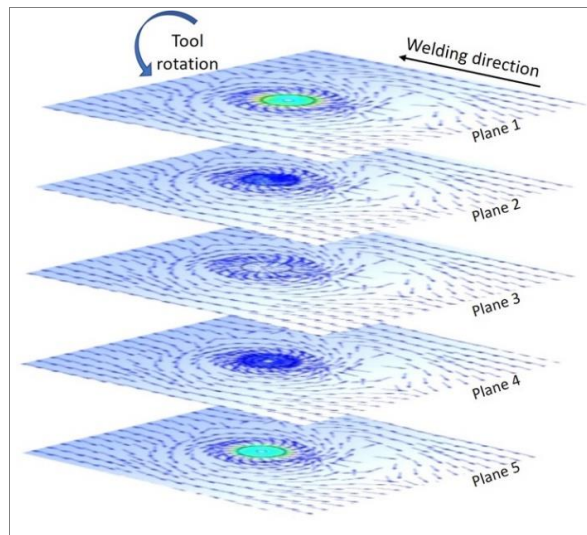


Figure 12.
Temperature contour of each plane corresponding to the planes defined in Figure 4

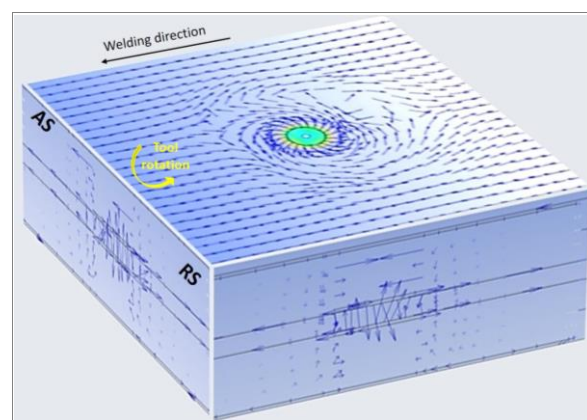


Figure 13.
Isometric view of material flow model

the surface farthest from the rotating shoulder [35], [36], reflecting less efficient heat distribution across the joint thickness.

Figure 13 shows isometric view of material flow contours which reveals a movement toward the plate's center thickness on both AS and RS, spanning upper and lower surfaces. This convergence is driven by three forces: shoulder compression into the plate, centrifugal force from tool rotation, and translational force along the welding direction. Together, they direct material toward the mid-thickness around the pin and the thermo-mechanically affected zone (TMAZ). This modeling study underscores the importance of maintaining symmetric heat input in the ODFSW process to achieve uniform material flow across the entire plate thickness. The similar velocity profiles observed at corresponding depths near the upper and lower surfaces indicate effective frictional heating and consistent material transport. At mid-thickness, opposing forces create random and turbulent material flow, producing fine, unoriented grains. This distinctive flow pattern highlights the process's complexity, where dual heat sources and

stirring mechanisms distinguish it from conventional FSW, offering advantages and challenges in achieving optimal weld quality.

The results in temperature control and material flow modeling in this One-Step Double-Acting Friction Stir Welding (ODFSW) process will have significant practical applications in industries where aluminum alloys are widely used, such as aerospace, automotive, and shipbuilding. Aluminum is a crucial material in these industries due to its high strength-to-weight ratio, corrosion resistance, and excellent thermal conductivity. In aerospace, aluminum alloys are essential for reducing aircraft weight while maintaining structural integrity. In automotive manufacturing, aluminum is increasingly used for lightweight vehicle components to improve fuel efficiency and crash performance. In shipbuilding, aluminum structures help reduce weight, enhance fuel efficiency, and improve corrosion resistance in marine environments. The ODFSW process enhances both productivity and joint properties, making it an attractive solution for these industries. Its ability to generate high-quality welds with minimal defects improves the mechanical performance of welded structures while increasing manufacturing efficiency. The process's unique double-acting mechanism allows for better material flow control, reducing defects like porosity and tunnel voids, which are critical in safety-sensitive applications. Furthermore, modeling plays a key role in predicting joint properties accurately, efficiently, and cost-effectively. Numerical simulations of temperature distribution and material flow enable manufacturers to optimize process parameters without the need for extensive experimental trials, reducing development costs and production time. This ensures that high-performance welds can be achieved consistently, meeting the stringent quality standards required in aerospace, automotive, and shipbuilding applications.

5. Conclusion

This study effectively validated the modeling of one-step double-acting FSW through both quantitative and qualitative approaches. Quantitative validation demonstrated a strong correlation between temperature predictions and Siddiqui's model, with an average error of just 4.07%.

Qualitative validation through microstructural grain orientation analysis confirmed the model's accuracy in predicting material flow patterns, particularly in the critical TMAZ region. The one-step double-acting FSW process exhibits a unique "double-V" thermal profile characterized by symmetrical and uniform heat distribution across the plate thickness. The dual-tool configuration generates peak temperatures near the outer surfaces, gradually decreasing toward the mid-thickness, ensuring effective solid-state welding. This unique thermal profile also leads to highly symmetric and uniform material flow throughout the plate thickness, facilitated by the dual-tool setup. Material velocity profiles are consistent near the top and bottom surfaces, with turbulence and finer grains observed at the mid-thickness due to opposing forces. This thermal and material flow symmetry contrasts with the single "V" profile of conventional FSW, which exhibits asymmetric heat distribution and material flow. Consequently, the one-step double-acting FSW process offers improved uniformity in heat input and material flow, reducing defects and enhancing joint quality.

Acknowledgements

The authors gratefully acknowledge the financial support provided by Universitas Sebelas Maret, Surakarta, Indonesia, through the Penelitian Kolaborasi Internasional grant, under contract number 194.2/UN27.22/PT.01.03/2024.

Authors' Declaration

Authors' contributions and responsibilities - The authors made substantial contributions to the conception and design of the study. The authors took responsibility for data analysis, interpretation, and discussion of results. The authors read and approved the final manuscript.

Funding – Universitas Sebelas Maret, Surakarta, Indonesia, through the Penelitian Kolaborasi Internasional grant, under contract number 194.2/UN27.22/PT.01.03/2024.

Availability of data and materials - All data is available from the authors.

Competing interests - The authors declare no competing interests.

Additional information – No additional information from the authors.

References

- [1] L. Dariusz and G. Pawel, "Estimation of Extrusion Welding Conditions for 6xxx Aluminum Alloys," *Procedia Manufacturing*, vol. 47, pp. 253–260, 2020, doi: 10.1016/j.promfg.2020.04.213.
- [2] E. D. W. S. Putri, A. R. Prabowo, N. Muhayat, and T. Triyono, "Application of Aluminum Alloys on Lightweight Vehicle Structure: Research Progress and Challenges," in *Lecture Notes in Mechanical Engineering*, 2024, pp. 109–113. doi: 10.1007/978-981-97-0106-3_17.
- [3] M. I. Hilmawan et al., "Effect of tools rotational speed on the mechanical properties of one-step double-acting friction stir welded aluminum alloy AA 6061 hollow panel," *International Journal of Lightweight Materials and Manufacture*, vol. 7, no. 3, pp. 467–479, May 2024, doi: 10.1016/j.ijlmm.2024.02.002.
- [4] D. W. Rathod, "A Review on challenges and opportunities in wire arc additive manufacturing of aluminium alloys: Specific context of 7xxx series alloys," *Mechanical Engineering for Society and Industry*, vol. 5, no. 1, 2025, doi: 10.31603/mesi.12711.
- [5] H. Granum, O. R. Myhr, T. Børvik, and O. S. Hopperstad, "Effect of pre-stretching on the mechanical behaviour of three artificially aged 6xxx series aluminium alloys," *Materials Today Communications*, vol. 27, p. 102408, Jun. 2021, doi: 10.1016/j.mtcomm.2021.102408.
- [6] Y. Wang, G. Zhao, L. Sun, X. Wang, D. Wei, and L. Liu, "Effects of welding angle on microstructure and mechanical properties of longitudinal weld in 6063 aluminum alloy extrusion profiles," *Journal of Materials Research and Technology*, vol. 17, pp. 756–773, Mar. 2022, doi: 10.1016/j.jmrt.2022.01.054.
- [7] S. Saifudin, N. Muhayat, E. Surojo, Y. H. Manurung, and T. Triyono, "Mitigation of Porosity and Residual Stress on Carbody Aluminum Alloy Vibration Welding: A Systematic Literature Review," *Automotive Experiences*, vol. 5, no. 3, pp. 477–493, Nov. 2022, doi: 10.31603/ae.7965.

- [8] B. F. Jogi, A. S. Awale, S. R. Nirantar, and H. S. Bhusare, "Metal Inert Gas (MIG) Welding Process Optimization using Teaching-Learning Based Optimization (TLBO) Algorithm," *Materials Today: Proceedings*, vol. 5, no. 2, pp. 7086–7095, 2018, doi: 10.1016/j.matpr.2017.11.373.
- [9] R. Kumar et al., "A comparative analysis of friction stir and tungsten inert gas dissimilar AA5082-AA7075 butt welds," *Materials Science for Energy Technologies*, vol. 5, pp. 74–80, 2022, doi: 10.1016/j.mset.2021.12.002.
- [10] T. Fiegl, M. Franke, A. Raza, E. Hryha, and C. Körner, "Effect of AlSi10Mg0.4 long-term reused powder in PBF-LB/M on the mechanical properties," *Materials & Design*, vol. 212, p. 110176, Dec. 2021, doi: 10.1016/j.matdes.2021.110176.
- [11] A. Hima Bindu, B. S. K. Chaitanya, K. Ajay, and I. Sudhakar, "Investigation on feasibility of dissimilar welding of AA2124 and AA7075 aluminium alloy using tungsten inert gas welding," *Materials Today: Proceedings*, vol. 26, pp. 2283–2288, 2020, doi: 10.1016/j.matpr.2020.02.494.
- [12] R. D. Ardika, T. Triyono, N. Muhayat, and Triyono, "A review porosity in aluminum welding," *Procedia Structural Integrity*, vol. 33, pp. 171–180, 2021, doi: 10.1016/j.prostr.2021.10.021.
- [13] Saifudin, N. Muhayat, E. Surojo, M. R. Muslih, and Triyono, "Effect of vibration frequency on mechanical properties and microstructure of metal inert gas welded dissimilar AA5083 and AA6061 aluminum alloy joints," *Results in Engineering*, vol. 24, p. 102970, Dec. 2024, doi: 10.1016/j.rineng.2024.102970.
- [14] Z. Afriansyah, M. Ashof, and A. Naimah, "Comparison of SMAW and GTAW Welding Properties," *Mechanics Exploration and Material Innovation*, vol. 1, no. 2, pp. 48–53, Apr. 2024, doi: 10.21776/ub.memi.2024.001.02.2.
- [15] S. Kotari, E. Punna, S. M. Gangadhar Reddy, and S. Venukumar, "Mechanical and micro structural behaviour of flux coated GTAW and FSW joined AA6061 aluminium alloy," *Materials Today: Proceedings*, vol. 27, pp. 1660–1667, 2020, doi: 10.1016/j.matpr.2020.03.562.
- [16] E. Sharghi and A. Farzadi, "Simulation of strain rate, material flow, and nugget shape during dissimilar friction stir welding of AA6061 aluminum alloy and Al-Mg₂Si composite," *Journal of Alloys and Compounds*, vol. 748, pp. 953–960, Jun. 2018, doi: 10.1016/j.jallcom.2018.03.145.
- [17] P. Kah, R. Rajan, J. Martikainen, and R. Suoranta, "Investigation of weld defects in friction-stir welding and fusion welding of aluminium alloys," *International Journal of Mechanical and Materials Engineering*, vol. 10, no. 1, p. 26, Dec. 2015, doi: 10.1186/s40712-015-0053-8.
- [18] D. B. Darmadi and M. Talice, "Improving the strength of friction stir welded joint by double side friction welding and varying pin geometry," *Engineering Science and Technology, an International Journal*, vol. 24, no. 3, pp. 637–647, Jun. 2021, doi: 10.1016/j.jestch.2020.11.001.
- [19] Hendrato, P. Puspitasari, Jamasri, and Triyono, "Fatigue crack growth rate and mechanical properties of one-step double-side friction stir welded AA6061-T6," *Results in Engineering*, vol. 21, p. 101958, Mar. 2024, doi: 10.1016/j.rineng.2024.101958.
- [20] S. Sivabalan, R. Sridhar, A. Parthiban, and G. Sathiskumar, "Experimental investigations of mechanical behavior of friction stir welding on aluminium alloy 6063," *Materials Today: Proceedings*, vol. 37, pp. 1678–1684, 2021, doi: 10.1016/j.matpr.2020.07.236.
- [21] H. Jia, K. Wu, and Y. Sun, "Numerical and experimental study on the thermal process, material flow and welding defects during high-speed friction stir welding," *Materials Today Communications*, vol. 31, p. 103526, Jun. 2022, doi: 10.1016/j.mtcomm.2022.103526.
- [22] F. R. Putra, A. S. Pramana, B. S. Pamungkas, R. Mauliyansyah, W. Suprpto, and A. A. J. Al-Hchaimi, "Effect of Stirring Time in Induction Furnace on Density, Porosity, Efficiency, Fluidity, and Geometry of Al-Mg-Si Castings," *Mechanics Exploration and Material Innovation*, vol. 1, no. 3, pp. 88–93, Jul. 2024, doi: 10.21776/ub.memi.2024.001.03.3.
- [23] D. Priyasudana et al., "Double side friction stir welding effect on mechanical properties and corrosion rate of aluminum alloy AA6061," *Heliyon*, vol. 9, no. 2, p. e13366, Feb. 2023, doi: 10.1016/j.heliyon.2023.e13366.
- [24] D. Ambrosio, Y. Morisada, K. Ushioda, and H. Fujii, "Material flow in friction stir welding: A review," *Journal of Materials Processing Technology*, vol. 320, p. 118116, Nov. 2023, doi: 10.1016/j.jmatprotec.2023.118116.

- [25] Y. Sharma, A. Mehta, H. Vasudev, N. Jeyaprakash, G. Prashar, and C. Prakash, "Analysis of friction stir welds using numerical modelling approach: a comprehensive review," *International Journal on Interactive Design and Manufacturing (IJIDeM)*, vol. 18, no. 8, pp. 5329–5342, Oct. 2024, doi: 10.1007/s12008-023-01324-6.
- [26] R. P. Youlia, W. Li, Y. Su, Y. Tang, and D. Utami, "Effectiveness and efficiency of tool alignment and simultaneity factors on double-sided friction stir welding for joining heat-treatable aluminum alloys: a review," *Welding in the World*, vol. 69, no. 2, pp. 407–430, Feb. 2025, doi: 10.1007/s40194-024-01867-6.
- [27] R. Mohan, J. U.B., and M. R., "CFD modelling of ultra-high rotational speed micro friction stir welding," *Journal of Manufacturing Processes*, vol. 64, pp. 1377–1386, Apr. 2021, doi: 10.1016/j.jmapro.2021.02.060.
- [28] Mohd Anees Siddiqui, S. A. H. Jafri, and Shahnawaz Alam, "Validation of Maximum Temperature during Friction Stir Welding of Butt Joint of Aluminium Alloy by using HyperWorks," *International Journal of Engineering Research and*, vol. V4, no. 04, Apr. 2015, doi: 10.17577/IJERTV4IS041182.
- [29] A. K. Kadian and P. Biswas, "A Comparative Study of Material Flow Behavior in Friction Stir Welding Using Laminar and Turbulent Models," *Journal of Materials Engineering and Performance*, vol. 24, no. 10, pp. 4119–4127, Oct. 2015, doi: 10.1007/s11665-015-1520-3.
- [30] O. P. Abolusoro, E. T. Akinlabi, and S. V. Kailas, "Tool rotational speed impact on temperature variations, mechanical properties and microstructure of friction stir welding of dissimilar high-strength aluminium alloys," *Journal of the Brazilian Society of Mechanical Sciences and Engineering*, vol. 42, no. 4, p. 176, Apr. 2020, doi: 10.1007/s40430-020-2259-9.
- [31] S. Chen et al., "Study on in-situ material flow behaviour during friction stir welding via a novel material tracing technology," *Journal of Materials Processing Technology*, vol. 297, p. 117205, Nov. 2021, doi: 10.1016/j.jmatprotec.2021.117205.
- [32] Y. Huang et al., "Material-flow behavior during friction-stir welding of 6082-T6 aluminum alloy," *The International Journal of Advanced Manufacturing Technology*, vol. 87, no. 1–4, pp. 1115–1123, Oct. 2016, doi: 10.1007/s00170-016-8603-7.
- [33] D. Zhang, P. Jiang, Q. Tang, Y. Lv, Q. Ran, and X. Chen, "Simulation of Material Flow Behavior during Friction Stir Welding of 7075 Aluminum Alloy," *Journal of Materials Engineering and Performance*, Jun. 2024, doi: 10.1007/s11665-024-09715-w.
- [34] D. G. Andrade, C. Leitão, N. Dialami, M. Chiumenti, and D. M. Rodrigues, "Modelling torque and temperature in friction stir welding of aluminium alloys," *International Journal of Mechanical Sciences*, vol. 182, p. 105725, Sep. 2020, doi: 10.1016/j.ijmecsci.2020.105725.
- [35] R. Jain, S. K. Pal, and S. B. Singh, "A study on the variation of forces and temperature in a friction stir welding process: A finite element approach," *Journal of Manufacturing Processes*, vol. 23, pp. 278–286, Aug. 2016, doi: 10.1016/j.jmapro.2016.04.008.
- [36] A. Silva-Magalhães, J. De Backer, J. Martin, and G. Bolmsjö, "In-situ temperature measurement in friction stir welding of thick section aluminium alloys," *Journal of Manufacturing Processes*, vol. 39, pp. 12–17, Mar. 2019, doi: 10.1016/j.jmapro.2019.02.001.
- [37] M. H. Miah, D. S. Chand, and G. S. Malhi, "Friction stir welding on temperature field for aluminum alloy based on combined HSM," *Materials Today: Proceedings*, vol. 56, pp. 675–680, 2022, doi: 10.1016/j.matpr.2022.01.101.
- [38] V. Pandian and S. Kannan, "Numerical prediction and experimental investigation of aerospace-grade dissimilar aluminium alloy by friction stir welding," *Journal of Manufacturing Processes*, vol. 54, pp. 99–108, Jun. 2020, doi: 10.1016/j.jmapro.2020.03.001.
- [39] Z. Sun and C. S. Wu, "Influence of tool thread pitch on material flow and thermal process in friction stir welding," *Journal of Materials Processing Technology*, vol. 275, p. 116281, Jan. 2020, doi: 10.1016/j.jmatprotec.2019.116281.